# Coherent control of boosted terahertz radiation from air plasma pumped by a femtosecond three-color sawtooth field

Shaojie Liu,[1] Zhengquan Fan,[1] Chenhui Lu,[2,*] Jieyu Gui,[1] Cheng Luo,[1] Shixiang Wang,[1] Qingqing Liang,[1] Bin Zhou,[1] Aurelién Houard,[3] André Mysyrowicz,[3] Vasily Kostin,[4,5] and Yi Liu[1,6,†]

[1]*Shanghai Key Lab of Modern Optical System, University of Shanghai for Science and Technology, Shanghai 200093, China*

[2]*School of Mechanical and Automotive Engineering, Shanghai University of Engineering Science, Shanghai 201620, China*

[3]*Laboratoire d'Optique Appliquée, ENSTA Paris, CNRS, Ecole Polytechnique, Institut Polytechnique de Paris, 828 Boulevard des Maréchaux, 91762 Palaiseau Cedex, France*

[4]*Institute of Applied Physics, Russian Academy of Sciences, Nizhny Novgorod 603950, Russia*

[5]*Scientific and Educational Mathematical Center, University of Nizhny Novgorod, Nizhny Novgorod 603950, Russia*

[6]*CAS Center for Excellence in Ultra-Intense Laser Science, Shanghai 201800, China*

(Received 8 September 2020; accepted 9 November 2020; published 15 December 2020)

We report on the coherent control of boosted ultrashort terahertz pulses emitted from air plasma pumped by a femtosecond sawtooth pulse composed of three optical harmonic fields. With an inline optical setup, the relative phases between the three optical components of the pump pulse can be varied independently with attosecond precision without the complexity of external phase stabilization. We observe that the amplitude of the terahertz emission pumped by the phase-optimized sawtooth wave is enhanced by 1.8 times compared to the widely used two-color scheme. Moreover, by manipulating the relative phases between the three colors at attosecond precision, coherent control of the azimuthal angle, ellipticity, and polarity of terahertz radiation is achieved. A local current model reproduces the coherent control observations well.

DOI: 10.1103/PhysRevA.102.063522

## I. INTRODUCTION

Air plasma created by ultrafast laser pulses is a unique source of coherent terahertz radiation because of its extremely broad bandwidth [1–4]. It reaches up to 200 THz, while other commonly used broadband THz radiation sources such as optical-conductive antenna or optical rectification crystals are usually limited to be below 5 THz [5–7]. It is well known that the combination of a fundamental femtosecond laser pulse with its second harmonic (two-color scheme) can produce THz radiation with a conversion efficiency of $10^{-4}$, two orders of magnitude higher than the single-color excitation [3,5,8–10]. With this two-color scheme, THz fields with amplitude exceeding 1 MV/cm have been demonstrated [11,12]. Moreover, the polarization and spectrum of the THz pulse can be controlled by varying the polarization, duration, and spectrum of the two-color pulses [13–19]. The THz generation mechanism has been first interpreted as a four-wave mixing process [2,13] and later attributed to a transient residual electron currents inside the plasma [3,9,16,19–22]. With a two-color optical driven field, a net transient transverse electron current is effectively produced, since the symmetric electron motion in the case of single-color pumping is broken [3,20–24]. Predicted in [23] and experimentally demonstrated in [24], THz generation by a two-color field with uncommon commensurate frequencies has confirmed that transient electron current is the dominating mechanism for such THz emission.

To further increase the terahertz yield, it was theoretically proposed to use three- and multicolor pumping fields [18,25]. Particularly, it was predicted that a sawtooth wave would be beneficial since such an optical field can increase the transient electron current by maximizing the electron drift velocity [25]. Numerical simulations show that terahertz energy can be significantly enhanced by such an engineered phase-optimized optical field [25–27]. The sawtoothlike wave can be synthesized by three or more optical fields with frequencies forming a series of harmonics, with their relative phase alternatively varied by $\pi$ [25]. Unfortunately, active control and stabilization of the relative phases between $N$-color optical fields ($N \geqslant 3$) in experiments are not all trivial and normally require complex feedback loops with attosecond control precision based on interferometer phase measurement [28,29]. Therefore THz generation using a femtosecond sawtoothlike wave has not yet been experimentally demonstrated, although THz enhancement has been observed with three-color fields obtained from an optical parametric amplifier (OPA), where the relative phases between the optical fields are usually not fixed [30,31].

In this work, we demonstrate a simple inline optical setup which enables attosecond control of the relative phases between three optical harmonic fields, without the need of any external phase stabilization system. Our method is based on the femtosecond laser pulses at 800-nm wavelength, which is widely available for the laboratories engaged in ultrafast optics. With optimized relative phases we find that the THz

*lchhuiz@163.com
†yi.liu@usst.edu.cn

 

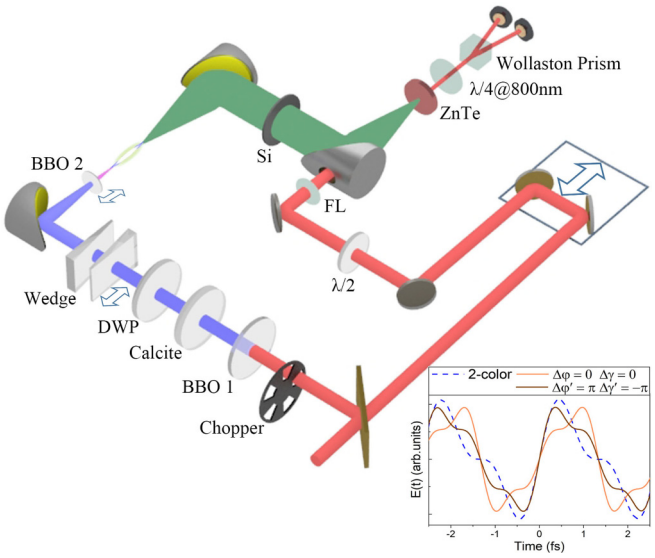


FIG. 1. Schematic experimental setup. The femtosecond laser pulses were split into pump and probe beams with a beam splitter. The BBO 1 and BBO 2 were used for second- and third-harmonic generation. The calcite plate cut at 90° imposes a negative group delay for the 800- and 400-nm pulse, in order to compensate the positive delay induced by other optical elements. The dual-wavelength plate (DWP) rotates the polarization plane of the 400 nm by 90° while keeping the polarization of the 800 nm unchanged. The insertion of the fused silica wedge was controlled by a mechanic motor. The THz radiation emitted by the air plasma was detected by the electrical-optical sampling system composed of the ZnTe crystal, the quarter wave plate, the Wollaston prism, and the balanced detector. Inset: The calculated synthesized laser field by two colors (gray line) and the sawtoothlike wave composed of three colors (red and blue lines).

pulse amplitude obtained with the three-color sawtoothlike wave is 1.8 times higher than that of two-color pumping. By adjusting the phases between the three colors, we show that this boosted terahertz emission can be coherently controlled in terms of azimuthal angle, polarity, and amplitude. We simulate this coherent control process with a local current model that reproduces the observations well. In particular, we show that the phase period for THz intensity variation now becomes $2\pi$ due to the absence of mirror symmetry of the sawtooth wave.

## II. SETUP FOR THE SAWTOOTHLIKE WAVE GENERATION AND TERAHERTZ FIELD DETECTION

For synthesis of the three-color femtosecond sawtoothlike wave, we used the optical setup schematically presented in Fig. 1. Femtosecond laser pulses first pass through a 200-$\mu$m-thick type-I beta barium borate (BBO) crystal cut at 29.2° for second-harmonics generation, which is followed by a calcite phase compensator, a dual-wavelength half-wave plate, and a pair of fused silica optical wedges. This optical layout is commonly used for two-color field coherent synthesis [32]. By displacing the fused silica wedges, the change of fused silica thickness $\Delta d$ induces a phase variation $\Delta\varphi = 2\pi(n_{800} - n_{400})\Delta d/\lambda_{400}$, where $n_{800}$ and $n_{400}$ are the refractive indices of fused silica for 800 and 400 nm wavelengths, respectively. It should be noticed that a change of transverse position of the moving wedges by $\Delta x = 10\,\mu$m results in a change of the wedge's thickness of $\Delta d = \Delta x \tan\theta = 0.524\,\mu$m, corresponding to $\Delta\varphi = 0.044\,\pi$. Here $\theta = 3°$ is the angle of the fused silica wedge. This leads to a time delay of 29.3 attoseconds between the 800- and 400-nm fields. Therefore $\Delta\varphi$ can be easily controlled with attosecond precision in this simple setup. The synchronized 800 and 400-nm fields, linearly polarized in the horizontal plane, are focused in air by a parabolic mirror. Before the focus, a 50-$\mu$m-thick type-I BBO crystal for sum-frequency generation (SFG) is inserted in the beam path in order to produce the third harmonics at 266 nm.

After the SFG crystal (BBO 2), the 800, 400, and 266 nm normally have both horizontal and vertical components due to the birefringence of the crystal. The relative phase between the 400 and 266 nm at the focus contains a constant phase component determined by the thickness of the BBO 2 and a variable phase $\gamma = 2\pi(n_{400}^{\text{air}} - n_{266}^{\text{air}}))l/\lambda_{266}$, where $l$ is the BBO-2-focus distance, and $n_{400}^{\text{air}}$ and $n_{266}^{\text{air}}$ are the refractive indices of air for 400-nm and 266-nm pulses. Therefore one can change the position of the BBO 2 to control $\gamma$. A change of $l$ by 10 $\mu$m corresponds to a phase change of $\Delta\gamma = 0.0011\,\pi$. In the Appendix we present a detailed consideration of the physical sources contributing to the phases $\varphi$ and $\gamma$. In the inset of Fig. 1 we present a comparison of a three-color sawtoothlike wave and the two-color wave to illustrate their difference.

Under the focusing role of the $f = 150$ mm parabolic mirror, the three-color wave was focused to form a plasma in air or nitrogen gas. Femtosecond pulses with 40-fs duration and pulse energy of 1.8 mJ before the first BBO crystal were used in the experiment. The emitted THz emission from the gas plasma was measured with the electronic-optical sampling (EOS) technique in a 1-mm-thick ZnTe crystal. By rotation of the detection crystal and the probe polarization, we can measure both horizontal and vertical components of the THz field. The experimental system was immersed in pure nitrogen to avoid the water vapor absorption of THz radiation.

## III. EXPERIMENTAL RESULTS

We first compared the THz emissions obtained by two-color and three-color sawtooth wave excitation. For the two-color case, the insertion of the fused silica wedge was optimized for the most intense THz generation [3]. The energy of the incident 800-nm pump pulse was 1.6 mJ, and the second harmonic was 0.2 mJ. The measured THz wave form is presented in Fig. 2(a) (red line). Since both 800- and 400-nm optical fields are linearly polarized in the horizontal plane [Fig. 3(a)], the resulting THz electric field is observed to be horizontally polarized with a weak vertical component, in agreement with previous results [13]. For the three-color field excitation, it is observed that both the rotation and azimuthal angle of the SFG crystal determine the intensity of the 266-nm field, as well as the polarization state of the exiting three optical fields. Moreover, the distance of the SFG BBO crystal with respect to the focus determines the phase $\Delta\gamma$. In a general case, the resulting THz emission exhibits both $x$ and $y$ components, with their amplitude and phase determined by

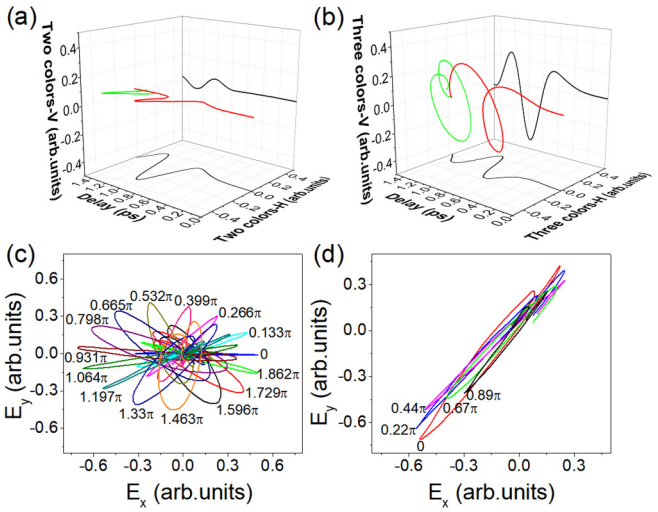


FIG. 2. (a), (b) Temporal wave form of the terahertz field produced by the two-color wave and sawtoothlike three-color wave. Both horizontal and vertical components of the THz electric field are presented. (c), (d) Trajectories of the THz electric field in the $x-y$ plane as a function of the phases $\Delta\varphi$ and $\Delta\gamma$.

the three-color optical fields. In the experiments, we optimize both the rotation and azimuth angle of the SFG crystal, as well as the relative phases $\Delta\varphi$ and $\Delta\gamma$, to achieve the most energetic THz emission. In Fig. 2(b) we present one such optimized THz field. The THz electric field now presents elliptical polarization with both horizontal and vertical components. The total amplitude of this optimized THz field is found to be 1.8 times higher than that of the two-color pumping, corresponding to an energy enhancement of 3.2 times. The corresponding polarizations of the 800-, 400-, and 266-nm optical fields are presented in Fig. 3(b).

We now examine the role of the relative phases $\Delta\varphi$ and $\Delta\gamma$. We present in Fig. 2(c) the profile of the THz electric field oscillation for a systematic variation of the phase $\Delta\varphi$. The azimuthal angle of the THz radiation, as well as its ellipticity, are observed to be controlled by this phase factor. The phase $\Delta\gamma$ was also changed by displacing the SFG crystal, and the resulting THz field profile is shown in Fig. 2(d). In this case, the THz field is found to be gently modified by the change of $\Delta\gamma$ in terms of the azimuthal angle and the ellipticity.

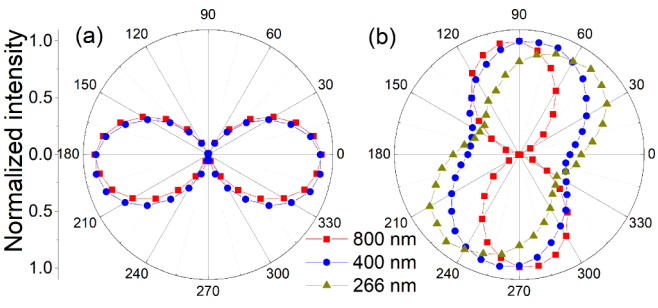


FIG. 3. Measurement of the polarization of the optical fields before (a) and after (b) the SFG BBO crystal. The energies of the 800-, 400-, and 266-nm pulses are measured as a function of the rotation angle of a Glan-Taylor polarizer.

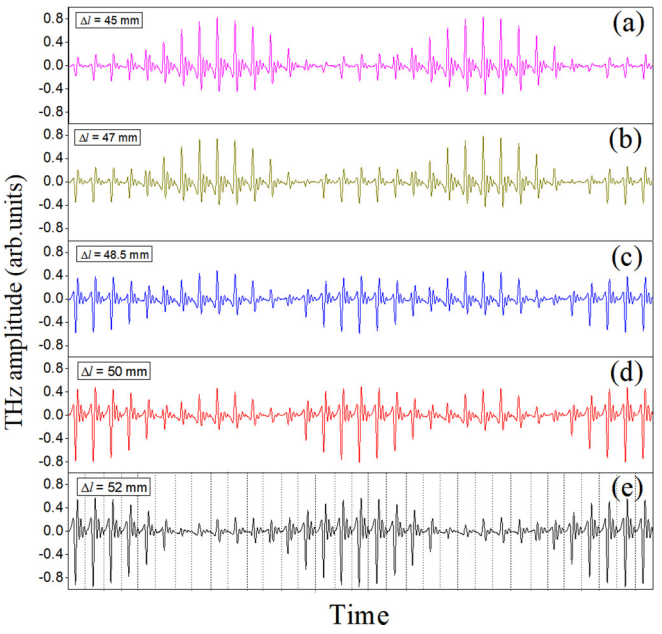


FIG. 4. Temporal wave form of the terahertz pulse as a function of the phase $\Delta\varphi$ for five different BBO-2-focus distances ($\Delta\gamma$). For (a)–(e), the BBO-2-focus distance was increased by an increment of 1.5 or 2 mm, corresponding to a $\Delta\gamma$ increment of $0.167\pi$ or $0.222\pi$. In each panel, 33 independent THz wave forms are presented for increasing $\Delta\varphi$ with an increment of $0.133\pi$ (0.03 mm of fused silica thickness). For each THz wave-form measurement, a temporal window of 3 ps has been presented. The square of the amplitude of the above THz wave forms are presented in Fig. 5(b) in the manuscript.

To get insight into the underlying physics mechanism and simplify the measurements, below we concentrate on one dimension of the THz field, namely, the vertically (y) polarized terahertz component. In Fig. 4 we present a systematic measurement of temporal wave form of the vertically polarized THz field in the time domain by varying $\Delta\varphi$, where five different $\Delta\gamma$ values were chosen. As seen, we coherently control the amplitude and polarity of the THz pulse by manipulation of $\Delta\varphi$. As an example, in Fig. 5(a) we present two representative THz wave forms with opposite polarities, achieved by $\Delta\varphi = 0$ and $\Delta\gamma = 0.78\pi$ versus $\Delta\varphi' = \pi$ and $\Delta\gamma' = 0.22\,\pi$. We present the squared modulus of THz peak-to-peak amplitude $|U_{\mathrm{THz}}|^2$, which is proportional to the THz pulse energy, as a function of $\Delta\varphi$ in Fig. 5(b). Here a $2\pi$-periodic variation of the THz energy is observed for all five different $\Delta\gamma$. The experimental results in Fig. 5(b) are well reproduced by numerical simulation, as presented in Fig. 5(c), which will be discussed later.

We next studied the role of $\Delta\gamma$, while the phase $\Delta\varphi$ was fixed at three chosen values. Systematic experimental results of the THz wave form are presented in Fig. 6. It is interesting to notice that the variation of BBO-2-focus distance ($\Delta\gamma$) does not necessary lead to a polarity change of the THz pulse, although its amplitude can be strongly modulated. We present in Fig. 7(a) the THz amplitude as a function of the BBO-2-focus distance. A periodic oscillation with a period of the BBO-2-to-focus distance of 18.0 mm was observed

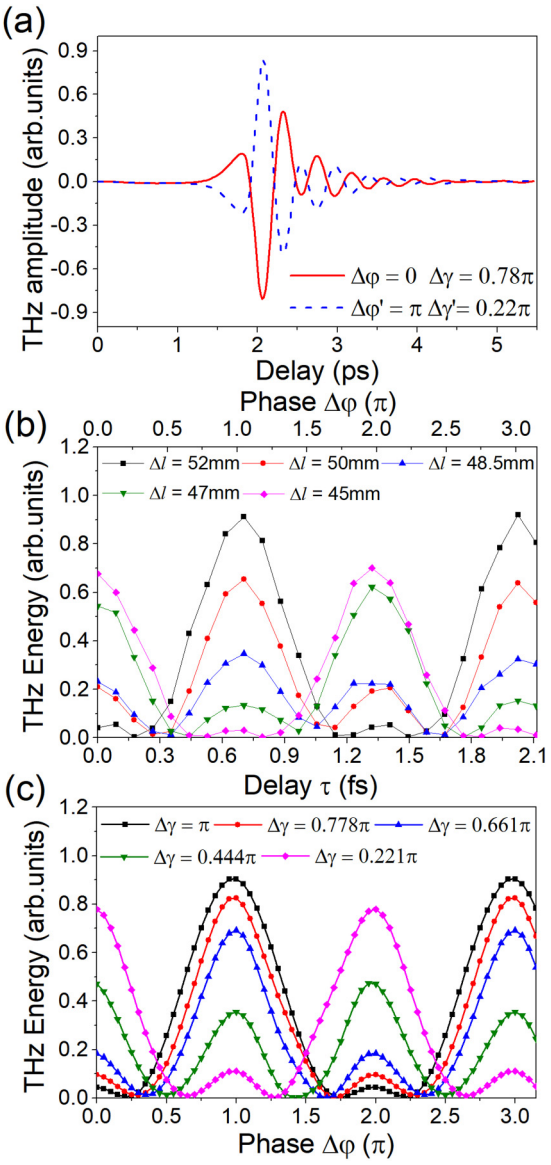


FIG. 5. (a) Experimental terahertz temporal wave forms with opposite polarities obtained with different combinations of $\Delta\varphi$ and $\Delta\gamma$. (b) Energy of the THz pulse as a function of the relative delay between the 800- and 400-nm laser field, while BBO-2-focus distance (corresponding to $\Delta\gamma$) was fixed at five different values. (c) THz energy from numerical simulations vs relative phase $\Delta\varphi$.

for all three chosen $\Delta\varphi$, corresponding to a $2\pi$ change of $\Delta\gamma$. The maximum THz amplitudes correspond to values of $\Delta\varphi$ differing by $n\pi (n = 0, \pm1, \pm2, ...)$, while the polarity of THz pulse remains unchanged for varying $\Delta\gamma$. For other values of $\Delta\varphi$, THz polarity change can also be observed, for example, in the case where $\tau = 0.352$ fs (corresponding to $\Delta\varphi = 0.53\,\pi$) as shown in Figs. 6(b) and 7(a).

## IV. DISCUSSION AND NUMERICAL SIMULATIONS

To corroborate our experimental findings, we utilized the local current (LC) model while neglecting the propagation effects [3,19,20,24,25]. The electric field projection $E(t)$ in a

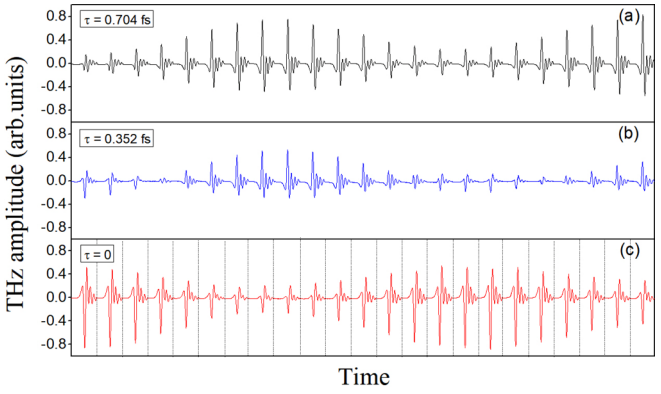


FIG. 6. Temporal wave form of the terahertz pulse as a function of the phase $\Delta\gamma$ for three different thicknesses of the fused silica wedge ($\Delta\varphi$). From (a) to (c), the thickness of the fused silica wedge was increased by an increment of 0.12 mm, corresponding to an increment of the time delay between the 800- and 400-nm pulse by 0.352 fs. In each panel, 23 independent THz wave forms are presented for increasing $\Delta\gamma$ with an increment of $0.111\pi$ by displacing the position of the BBO 2 with respect to the focus by $\Delta l$ of 1 mm. For each THz wave-form measurements, a temporal window of 3 ps has been presented. The amplitude of the above THz wave forms is presented in Fig. 7(a) in the manuscript.

linearly polarized three-color laser pulse is expressed as

$$E(t) = \exp\left(\frac{-2\ln 2t^2}{\tau^2}\right)[E_{800}\sin(\omega_0 t) + E_{400}\sin(2\omega_0 t + \pi + \Delta\varphi) + E_{266}\sin(3\omega_0 t + \Delta\varphi + \Delta\gamma)], \quad (1)$$

where $t$ is the time variable, $\tau$ is the intensity FWHM, and $\omega_0 = 2\pi c/\lambda_{800}$ is the fundamental frequency. $E_{800}$, $E_{400}$, and $E_{266}$ are the field amplitudes of the fundamental, second-, and third-harmonic laser field, respectively. More details concerning Eq. (1) can be found in the Appendix. For a standard sawtoothlike pulse, the amplitude ratios should be set to $E_{400} = E_{800}/2$ and $E_{266} = E_{800}/3$ and the phase shifts $\Delta\varphi$ and $\Delta\gamma$ should be set to zeros. In our experiment, the pulse energies of the 400- and 266-nm pulses are measured to be 230 and 22.5 $\mu$J, respectively. However, due to the intensity clamping effect inside the plasma for the fundamental 800 nm pulse and the strong defocusing effect of the plasma on the 400- and 266-nm pulses, the precise laser intensities of the three optical pulses cannot be identified easily. Therefore, in our simulations, we have tested a vast range of laser intensity ratio between the three optical fields, and we found the best agreement between experiments and simulations is obtained in the case of $E_{400} = E_{800}/4$ and $E_{266} = E_{800}/5$.

For the fundamental laser intensities in our experimental conditions ($10^{14}$–$10^{15}$ W/cm$^2$), the tunneling formula can be employed to calculate the ionization rate $W(t)$ [33]:

$$W(t) = \frac{\alpha}{|\varepsilon(t)|}\exp\left[-\left(\frac{\beta}{|\varepsilon(t)|}\right)\right], \quad (2)$$

where $\varepsilon(t) = E(t)/\varepsilon_a$ is the electric field in atomic units, with $\varepsilon_a = 5.14 \times 10^9$ V/cm, $\alpha = 4\omega_a r^{5/2}$, $\beta = (2/3)r^{3/2}$, $\omega_a = 4.13 \times 10^{16}$ s$^{-1}$ as the atomic frequency, and $r$ is the ioniza-

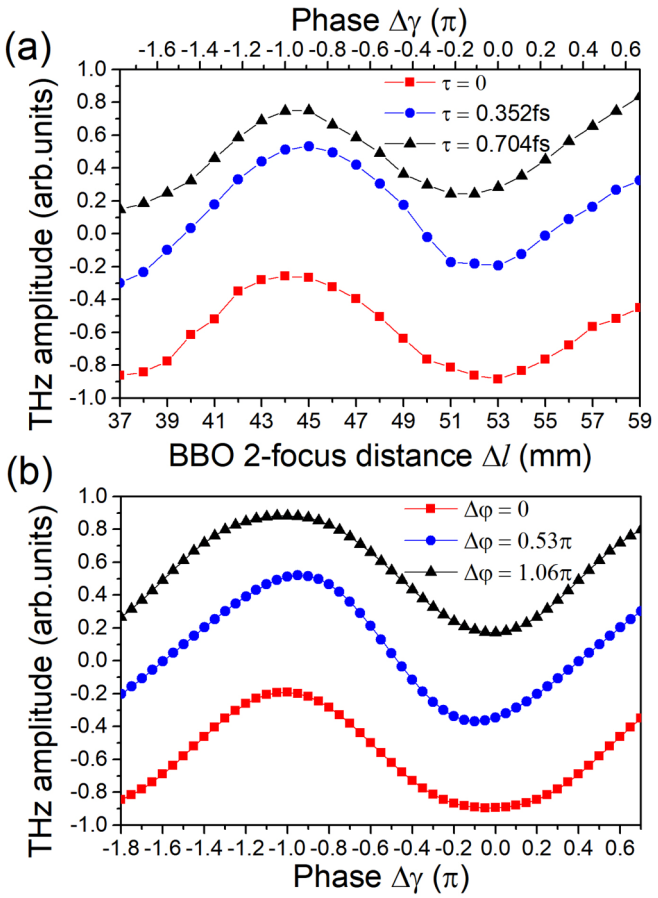


FIG. 7. (a) Amplitude of the THz pulse as a function of the BBO-2-focus distance $\Delta l$ defining $\Delta\gamma$, with delay $\tau$ (corresponding to phase $\Delta\varphi$) fixed at three different values. (b) THz amplitude from numerical simulations vs relative phase $\Delta\gamma$.

tion potential of the gas molecule relative to hydrogen atom $r = U/U^H$. In our simulations we used $U = 15.6\,\text{eV}$ (for $N_2$ gas) and $U^H = 13.6\,\text{eV}$. The free electron density $N_e(t)$ can be written as

$$\frac{dN_e(t)}{dt} = W(t)[N - N_e(t)], \tag{3}$$

where $N$ is the initial density of neutral gas. Considering the movement of all ionized electrons, the generated transverse electron current can be expressed as

$$J(t) = e\int_{-\infty}^{t} v(t,t')dN_e(t'), \tag{4}$$

where $e$ is the elementary charge, $dN_e(t')$ represents the change of the electron density in the interval between $t'$ and $t' + dt'$, $v(t,t') = -\frac{e}{m}\int_{t'}^{t} dt'' E(t'')\exp[-\nu(t-t'')]$ can be seen as the velocity of an electron at time instant $t$, which is born at the ionization instant $t'$, and $\nu$ is the phenomenological collision rate ($\nu \approx 5\,\text{ps}^{-1}$). The time-dependent electron current $J(t)$ generates an electromagnetic pulse at THz frequencies. The electric field of the generated THz pulse is proportional to the derivative of the electron current $J(t)$:

$$E_{\text{THz}}(t) \propto \frac{d}{dt}[J(t)]. \tag{5}$$

Finally, the THz radiation spectrum is obtained by the Fourier transform of $E_{\text{THz}}(t)$, i.e., $E_{\text{THz}}(\omega) = \text{FFT}[E_{\text{THz}}(t)]$. The THz yield is calculated as $U_{\text{THz}} \propto \int_0^{\omega_{th}} E^2_{\text{THz}}(\omega)d\omega$, where $\omega_{\text{th}} = 100\,\text{THz}$ is the upper limit of the THz spectrum considered in our simulation.

In Fig. 5(c) we present the calculated THz yield as a function of the relative phase $\Delta\varphi$. As can be seen, the dependence agrees quantitatively with the experimental results shown in Fig. 5(b). The intensity variation period is $2\pi$, instead of the period of $\pi$ observed in the two-color pumping situation [13,20]. This is due to the fact that a change of $\Delta\varphi$ by $\pi$ leads to a mirror symmetrical synthesized laser field in the case of two-color excitation. As a result, this leads to a polarity-inversed THz wave form of identical amplitude, which corresponds to the same THz energy [13,32]. In the situation of three-color sawtoothlike wave pumping, when $\Delta\varphi$ is changed by $\pi$ the THz amplitude becomes different, since the 266-nm field breaks the mirror symmetry of the 800- and 400-nm field. Consequently, the variation period in Fig. 5(c) becomes $2\pi$. We noticed that the maximum THz energy is achieved when both $\Delta\varphi$ and $\Delta\gamma$ are equal to $m\pi\,(m = 0, \pm1, \pm2, ...)$. In Fig. 7(b), the simulated THz amplitude is compared with the experimental results, where a good agreement is also obtained. Based on a similar analysis, the period with respect to $\Delta\gamma$ is also $2\pi$.

## V. CONCLUSION

In conclusion, we demonstrated a simple and robust inline optical setup enabling precise control of the relative phases between three harmonic femtosecond laser fields, providing a sawtoothlike wave. It is based on the widely available femtosecond laser pulses at 800 nm. It was observed that the THz radiation amplitude produced in air with this phase-optimized three-color sawtoothlike wave is enhanced by 80% compared to that produced with two-color laser fields. The coherent control of azimuth angle, polarity, and amplitude of the enhanced THz pulse through a variation of the relative phases $\Delta\varphi$ or $\Delta\gamma$ of the three-color fields is in good agreement with the transient electron current model. Well-controlled production of intense THz pulses of ultrashort duration (close to a single-cycle pulse) and concomitant broadband spectrum should be beneficial for ultrafast dynamics application in the THz domain. Moreover, this simple and robust three-color optical field synthesizer with attosecond precision can find wide applications in the domain of femtosecond laser-material interaction, such as high-order harmonic generation [34,35], generation of white-light continuum in the mid-IR and UV regime [36–38], and field-free molecule alignment and orientation [39], where three-color femtosecond pulse excitation has been found to be much more efficient and beneficial.

## ACKNOWLEDGMENTS

We acknowledge the support of the National Natural Science Foundation of China (Grants No. 12034013, No. 11604205, and No. 11904232), the Innovation Program of the Shanghai Municipal Education Commission (Grant No. 2017-01-07-00-07-E00007), and the Shanghai Municipal Science and Technology Commission (Grant No. 19560745800).

V.K. acknowledges support from the Russian Science Foundation (Grant No. 18-11-00210). C.L. acknowledges support from the Talent Program of Shanghai University of Engineering Science.

## APPENDIX: PHASE RELATIONSHIP BETWEEN THE THREE-COLOR LASER FIELDS

In this Appendix we introduce the expression (1) used in the manuscript and describe the relationship between the phase terms and the experimental parameters. First we introduce the expression for the three-color laser field at the focus with our optical layout. Considering the optical setup in Fig. 1 of the manuscript, the laser field can be written as

$$E(t) = \exp\left(\frac{-2\ln 2t^2}{\tau^2}\right)[E_{800}\sin(\omega_0 t) + E_{400}\sin(2\omega_0 t + \varphi + \alpha) + E_{266}\sin(3\omega_0 t + \varphi + \beta + \gamma)]. \quad \text{(A1)}$$

Here $t$ is the time variable, $\tau$ is the intensity FWHM, $\omega_0 = 2\pi c/\lambda_{800}$ is the fundamental frequency. $E_{800}$, $E_{400}$, and $E_{266}$ are the amplitude of the fundamental, second, and third harmonics. Now we explain the phase terms.

(i) The phase $\varphi$ denotes the phase difference between the 400- and 800-nm field introduced by the movable fused silica wedge. It is related to the thickness $d$ of the wedge by $\varphi = 2\pi(n_{400} - n_{800})d/\lambda_{400}$, where $n_{400}$ and $n_{800}$ are the refractive indices of fused silica for 400- and 800-nm light pulses.

(ii) The phase $\alpha$ presents the phase difference introduced by all other transmission elements from the BBO 1 to the focus. Five elements contribute to this phase difference: (1) the second-harmonic generation crystal (BBO 1), (2) the calcite plate, (3) the dual-wavelength plate, (4) the sum-frequency generation crystal (BBO 2), and (5) the optical pass in air between the BBO 1 and the focus. For a given BBO-1-focus distance (the case of all our experiments), the above five contributions of the phase difference are constant. Therefore it can be represented by a phase term $\alpha$.

(iii) For the sum-frequency generation inside the second BBO crystal, the phase difference $\varphi$ will be transferred to the 266-nm pulse accompanying the SFG generation. Therefore in the phase of the 266-nm field there also exists the term $\varphi$.

(iv) There are two other elements contributing to the relative phase of the 266-nm laser field. The first element is the SFG crystal (BBO 2), which introduces a phase constant $\beta$ determined by the BBO thickness. The second contribution is the optical pass in air between the rear surface of BBO 2 and the focus. The second contribution can be expressed as $\gamma = 2\pi(n_{400}^{\text{air}} - n_{266}^{\text{air}})l/\lambda_{266}$, where $l$ is the BBO 2-focus distance, and $n_{400}^{\text{air}}$ and $n_{266}^{\text{air}}$ are the refractive indices of air for 400-nm and 266-nm pulses. Therefore one can change the position of the BBO 2 to control $\gamma$. A change of $l$ by 10 $\mu$m corresponds to a phase change of $\Delta\gamma = 0.0011\,\pi$.

In view that $\alpha$ and $\beta$ are both constant in our experiments and that $\varphi$ and $\gamma$ are variables, in order to write the expression of electric field to be compatible with that of the sawtooth wave in Ref. [25], we can always choose special $\varphi_0$ and $\gamma_0$ to fulfill the following relationship:

$$\varphi_0 + \alpha = \pi, \quad \text{(A2)}$$

$$\varphi_0 + \gamma_0 + \beta = 0. \quad \text{(A3)}$$

In this case the phase change induced by translation of the optical wedge or displacement of the BBO 2 can be expressed as

$$\Delta\varphi = \varphi - \varphi_0, \quad \text{(A4)}$$

$$\Delta\gamma = \gamma - \gamma_0. \quad \text{(A5)}$$

As a result, the electric field now reads

$$E(t) = \exp\left(\frac{-2\ln 2t^2}{\tau^2}\right)[E_{800}\sin(\omega_0 t) + E_{400}\sin(2\omega_0 t + \pi + \Delta\varphi) + E_{266}\sin(3\omega_0 t + \Delta\varphi + \Delta\gamma)]. \quad \text{(A6)}$$

[1] H. Hamster, A. Sullivan, S. Gordon, W. White, and R. W. Falcone, Subpicosecond, Electromagnetic Pulses from Intense Laser-Plasma Interaction, Phys. Rev. Lett. **71**, 2725 (1993).

[2] D. J. Cook and R. M. Hochstrasser, Intense terahertz pulses by four-wave rectification in air, Opt. Lett. **25**, 1210 (2000).

[3] K. Y. Kim, A. J. Taylor, J. H. Glownia, and G. Rodriguez, Coherent control of terahertz supercontinuum generation in ultrafast laser–gas interactions, Nat. Photonics **2**, 605 (2008).

[4] E. Matsubara, M. Nagai, and M. Ashida, Ultrabroadband coherent electric field from far infrared to 200 THz using air plasma induced by 10 fs pulses, Appl. Phys. Lett. **101**, 011105 (2012).

[5] A. Nahata, A. S. Weling, and T. F. Heinz, A wideband coherent terahertz spectroscopy system using optical rectification and electrooptic sampling, Appl. Phys. Lett. **69**, 2321 (1996).

[6] Q. Wu and X.-C. Zhang, Freespace electrooptic sampling of terahertz beams, Appl. Phys. Lett. **67**, 3523 (1995).

[7] T. Löffler, M. Kreß, M. Thomson, T. Hahn, N. Hasegawa, and H. G. Roskos, Comparative performance of terahertz emitters in amplifier-laser-based systems, Semicond. Sci. Technol. **20**, S134 (2005).

[8] C. D'Amico, A. Houard, M. Franco, B. Prade, A. Mysyrowicz, A. Couairon, and V. T. Tikhonchuk, Conical Forward THz Emission from Femtosecond-Laser-Beam Filamentation in Air, Phys. Rev. Lett. **98**, 235002 (2007).

[9] T. I. Oh, Y. S. You, N. Jhajj, E. W. Rosenthal, H. M. Milchberg, and K. Y. Kim, Intense terahertz generation in two-color laser

filamentation: Energy scaling with terawatt laser systems, New J. Phys. **15**, 075002 (2013).

[10] I. Babushkin, W. Kuehn, C. Köhler, S. Skupin, L. Bergé, K. Reimann, M. Woerner, J. Herrmann, and T. Elsaesser, Ultrafast Spatiotemporal Dynamics of Terahertz Generation by Ionizing Two-Color Femtosecond Pulses in Gases, Phys. Rev. Lett. **105**, 053903 (2010).

[11] Y.-J. Yoo, D. Jang, and K.-Y. Kim, Highly enhanced terahertz conversion by two-color laser filamentation at low gas pressures, Opt. Express **27**, 22663 (2019).

[12] Y.-J. Yoo, D, Kuk, Z, Zhong, and K.-Y. Kim, Generation and characterization of strong terahertz fields from kHz laser filamentation, IEEE J. Sel. Top. Quantum Electron. **23**, 8501007 (2017).

[13] X. Xie, J. Dai, and X.-C. Zhang, Coherent Control of THz Wave Generation in Ambient Air, Phys. Rev. Lett. **96**, 075005 (2006).

[14] H. Wen and A. M. Lindenberg, Coherent Terahertz Polarization Control through Manipulation of Electron Trajectories, Phys. Rev. Lett. **103**, 023902 (2009).

[15] J. Dai, N. Karpowicz, and X.-C. Zhang, Coherent Polarization Control of Terahertz Waves Generated From Two-Color Laser-Induced Gas Plasma, Phys. Rev. Lett. **103**, 023001 (2009).

[16] Z. Zhang, Y. Chen, S. Cui, F. He, M. Chen, Z. Zhang, J. Yu, L. Chen, Z. Sheng, and J. Zhang, Manipulation of polarizations for broadband terahertz waves emitted from laser plasma filaments, Nat. Photonics **12**, 554 (2018).

[17] F. Théberge, M. Châteauneuf, G. Roy, P. Mathieu, and J. Dubois, Generation of tunable and broadband far-infrared laser pulses during two-color filamentation, Phys. Rev. A **81**, 033821 (2010).

[18] I. Babushkin, S. Skupin, A. Husakou, C. Köhler, E. Cabrera-Granado, L. Bergé, and J. Herrmann, Tailoring terahertz radiation by controlling tunnel photoionization events in gases, New J. Phys. **13**, 123029 (2011).

[19] N. V. Vvedenskii, A. I. Korytin, V. A. Kostin, A. A. Murzanev, A. A. Silaev, and A. N. Stepanov, Two-Color Laser-Plasma Generation of Terahertz Radiation Using a Frequency-Tunable Half Harmonic of a Femtosecond Pulse, Phys. Rev. Lett. **112**, 055004 (2014).

[20] K. Y. Kim, J. H. Glownia, A. J. Taylor, and G. Rodriguez, Terahertz emission from ultrafast ionizing air in symmetry-broken laser fields, Opt. Express **15**, 4577 (2007).

[21] V. A. Andreeva, O. G. Kosareva, N. A. Panov, D. E. Shipilo, P. M. Solyankin, M. N. Esaulkov, P. González de Alaiza Martínez, A. P. Shkurinov, V. A. Makarov, L. Bergé, and S. L. Chin, Ultrabroad Terahertz Spectrum Generation from an Air-Based Filament Plasma, Phys. Rev. Lett. **116**, 063902 (2016).

[22] L. Bergé, S. Skupin, C. Köhler, I. Babushkin, and J. Herrmann, 3D Numerical Simulations of THz Generation by Two-Color Laser Filaments, Phys. Rev. Lett. **110**, 073901 (2013).

[23] V. A. Kostin, I. D. Laryushin, A. A. Silaev, and N. V. Vvedenskii, Ionization-Induced Multiwave Mixing: Terahertz Generation with Two-Color Laser Pulses of Various Frequency Ratios, Phys. Rev. Lett. **117**, 035003 (2016).

[24] L.-L. Zhang, W.-M. Wang, T. Wu, R. Zhang, S.-J. Zhang, C.-L. Zhang, Y. Zhang, Z.-M. Sheng, and X.-C. Zhang, Observation of Terahertz Radiation via the Two-Color Laser Scheme with Uncommon Frequency Ratios, Phys. Rev. Lett. **119**, 235001 (2017).

[25] P. González de Alaiza Martínez, I. Babushkin, L. Bergé, S. Skupin, E. Cabrera-Granado, C. Köhler, U. Morgner, A. Husakou, and J. Herrmann, Boosting Terahertz Generation in Laser-Field Ionized Gases Using a Sawtooth Wave Shape, Phys. Rev. Lett. **114**, 183901 (2015).

[26] C. Lu, C. Zhang, L. Zhang, X. Wang, and S. Zhang, Modulation of terahertz-spectrum generation from an air plasma by tunable three-color laser pulses, Phys. Rev. A **96**, 053402 (2017).

[27] V. A. Kostin, I. D. Laryushin, and N. V. Vvedenskii, Generation of terahertz radiation by multicolor ionizing pulses, JETP Lett. **112**, 77 (2020).

[28] A. Wirth, M. Th. Hassan, I. Grguraš, J. Gagnon, A. Moulet, T. T. Luu, S. Pabst, R. Santra, Z. A. Alahmed, A. M. Azzeer, V. S. Yakovlev, V. Pervak, F. Krausz, and E. Goulielmakis, Synthesized light transients, Science **334**, 195 (2001).

[29] C. Burger, W. F. Frisch, T. M. Kardaś, M. Trubetskov, V. Pervak, R. Moshammer, B. Bergues, M. F. Kling, and P. Wnuk, Compact and flexible harmonic generator and three-color synthesizer for femtosecond coherent control and time-resolved studies, Opt. Express **25**, 31130 (2017).

[30] V. Vaičaitis, O. Balachninaitė, U. Morgner, and I. Babushkin, Terahertz radiation generation by three-color laser pulses in air filament, J. Appl. Phys. **125**, 173103 (2019).

[31] J. D. Bagley, C. D. Moss, S. A. Sorenson, and J. A. Johnson, Laser-induced plasma generation of terahertz radiation using three incommensurate wavelengths, J. Phys. B **51**, 144004 (2018).

[32] J. Dai and X.-C. Zhang, Terahertz wave generation from gas plasma using a phase compensator with attosecond phase-control accuracy, Appl. Phys. Lett. **94**, 021117 (2009).

[33] P. B. Corkum, N. H. Burnett, and F. Brunel, Above Threshold Ionization in the Long Wavelength Limit, Phys. Rev. Lett. **62**, 1259 (1989).

[34] P. Wei, J. Miao, Z. Zeng, C. Li, X. Ge, R. Li, and Z. Xu, Selective Enhancement of a Single Harmonic Emission in a Driving Laser Field with Subcycle Waveform Control, Phys. Rev. Lett. **110**, 233903 (2013).

[35] C. Jin, G. Wang, H. Wei, A.-T. Le, and C. D. Lin, Waveforms for optimal sub-keV high-order harmonics with synthesized two- or three-colour laser fields, Nat. Commun. **5**, 4003 (2014).

[36] P. B. Petersen and A. Tokmakoff, Source for ultrafast continuum infrared and terahertz radiation, Opt. Lett. **35**, 1962 (2010).

[37] Y. Kida, K. Sakamoto, and T. Imasaka, High-energy multicolor femtosecond pulses in the deep-ultraviolet generated through four-wave mixing induced by three-color pulses, Appl. Phys. B **122**, 214 (2016).

[38] V. A. Kostin and N. V. Vvedenskii, Generation of Few- and Subcycle Radiation in Midinfrared-to-Deep-Ultraviolet Range During Plasma Production by Multicolor Femtosecond Pulses, Phys. Rev. Lett. **120**, 065002 (2018).

[39] S. Zhang, J. Shi, H. Zhang, T. Jia, Z. Wang, and Z. Sun, Field-free molecular orientation by a multicolor laser field, Phys. Rev. A **83**, 023416 (2011).